Abundances, emissions, and loss processes of the long-lived and potent greenhouse gas octafluorooxolane (octafluorotetrahydrofuran, c-C_4F_8O) in the atmosphere

Martin K. Vollmer[1], François Bernard[2,3,4], Blagoj Mitrevski[5], L. Paul Steele[5], Cathy M. Trudinger[5], Stefan Reimann[1], Ray L. Langenfelds[5], Paul B. Krummel[5], Paul J. Fraser[5], David M. Etheridge[5], Marc A. J. Curran[6,7], and James B. Burkholder[2]

[1]Laboratory for Air Pollution and Environmental Technology, Empa, Swiss Federal Laboratories for Materials Science and Technology, Überlandstrasse 129, 8600 Dübendorf, Switzerland
[2]Earth System Research Laboratory, NOAA, National Oceanic and Atmospheric Administration, Boulder, Colorado, USA
[3]Cooperative Institute for Research in Environmental Sciences, University of Colorado, Boulder, Colorado, USA
[4]now at: Institut de Combustion Aérothermique, Réactivité et Environnement, Centre National de la Recherche Scientifique, Observatoire des Sciences de l'Univers en région Centre, Orléans, France
[5]Climate Science Centre, CSIRO Oceans and Atmosphere, Aspendale, Victoria, Australia
[6]Australian Antarctic Division, 203 Channel Highway, Kingston, Tasmania 7050, Australia
[7]Antarctic Climate & Ecosystems Cooperative Research Centre, Hobart, Tasmania 7001, Australia

Correspondence to: Martin K. Vollmer (martin.vollmer@empa.ch)

Abstract. The first observations of octafluorooxolane (octafluorotetrahydrofuran, c-C_4F_8O), a persistent greenhouse gas, in the atmosphere are reported. In addition, a complimentary laboratory study of its most likely atmospheric loss processes and infrared absorption spectrum and global warming potential (GWP) are reported. First atmospheric measurements of c-C_4F_8O are provided from the Cape Grim Air Archive (41°S, Tasmania, Australia, 1978–present), supplemented by two firn air samples

5   from Antarctica, in situ measurements of ambient air at Aspendale, Victoria (38°S), and a few archived air samples from the Northern Hemisphere. Atmospheric abundances in the Southern Hemisphere have reached 74 ppq (parts per quadrillion, femtomol mol^{-1} in dry air) by 2017. However its growth rate has decreased from a maximum in 2004 of 4.3 ppq yr^{-1} to <0.15 ppq yr^{-1} in 2017. Using a 12-box atmospheric transport model, globally averaged yearly emissions and abundances of c-C_4F_8O are calculated for 1951–2017. Emissions, which we speculate to derive predominantly from usage of c-C_4F_8O as a

10   solvent in the semiconductor industry, peaked at 0.16 ($\pm$0.04, 2σ) kt yr^{-1} in 2004 and have after declined to <0.01 kt yr^{-1} in 2017. Cumulative emissions over the full range of our record amount to 2.8 (2.6–3.2) kt, which correspond to 34 Mt of CO_2-equivalent emissions. Infrared and ultraviolet absorption spectra for c-C_4F_8O as well as the reactive channel rate coefficient for the O(^{1}D) + c-C_4F_8O reaction were determined from laboratory studies. On the basis of these experiments, a radiative efficiency of 0.430 W m^{-2} ppb^{-1} (parts per billion, nanomol mol^{-1}) was determined, which is one of the largest found for

15   synthetic greenhouse gases. The global annually averaged atmospheric lifetime, including mesospheric loss, is estimated to be >3 000 years. GWPs of 8 975, 12 000, and 16 000 are estimated for the 20, 100, and 500-year time-horizons, respectively.

1 Introduction

Halogenated organic substances are generally potent greenhouse gases and contribute significantly to climate change, despite their relatively low abundances in the atmosphere (Myhre et al., 2013; Carpenter and Reimann, 2014). Hydrofluorocarbons (HFCs), perfluorocarbons (PFCs), sulfur hexafluoride and nitrogen trifluoride (NF$_3$) are important anthropogenic greenhouse

5 gases, which are included in the Kyoto Protocol to the United Nations' Framework Convention on Climate Change (UNFCCC). Although they don't have the capacity to destroy stratospheric ozone (unlike e.g. chlorofluorocarbons), HFCs have also been added to the Montreal Protocol That Deplete the Ozone Layer through the recent Kigali Amendment (United Nations, 2016).

The topic of the present research is the heterocyclic and fully fluorinated compound octafluorooxolane (c-C$_4$F$_8$O, CAS 773-14-8), better known by its older name as octafluorotetrahydrofuran, from which it has recently been renamed to its present

10 name by IUPAC (Favre and Powell, 2014). The compound is not regulated under the above Protocols despite its potential long lifetime and high radiative efficiency.

c-C$_4$F$_8$O has been under discussion in the recent literature foremost as a new Chemical Vapor Deposition (CVD) chamber cleaning agent in the semiconductor industry (Pruette et al., 2000; McCoy, 2000; Oh et al., 2001; Kim et al., 2002, 2004). It was evaluated against the widely used perfluoroethane (C$_2$F$_6$) and perfluoropropane in terms of cleaning effectiveness and reduction

15 in greenhouse gas emissions. Its advantages over NF$_3$, another alternative cleaning agent, are stated as lower toxicity and a smaller adjustment to existing chamber cleaning structures using C$_2$F$_6$. However, its disadvantages are potential byproducts such as tetrafluoromethane, which is another long-lived potent greenhouse gas (Beu, 2005). c-C$_4$F$_8$O has also been evaluated as part of a gas mixture to replace SF$_6$ in high-voltage gaseous insulation applications, again driven by the desire to reduce greenhouse gas emissions (Dahl et al., 2014; Chachereau et al., 2016). Another niche application is the use as a radiator gas

20 for Cherenkov detectors in large scale particle acceleration experiments (Artuso et al., 2006; Acconcia et al., 2014).

The above applications have emerged only within the last two decades. Whether c-C$_4$F$_8$O was used earlier than that is undocumented. Frick and Anderson (1972) patented a method to synthesize c-C$_4$F$_8$O for potential use as an inert solvent for highly reactive or corrosive halogenated materials in naval applications. However it remains unclear if this led to mass production of c-C$_4$F$_8$O at that time.

25 Little is known of the c-C$_4$F$_8$O properties related to radiative properties and gas phase loss processes in the atmosphere. As part of the above-mentioned evaluations, a greenhouse warming potential (GWP) is cited at a value of 8 700 (with no reference to the time horizon) and was derived based on structural analogies to octafluorocyclobutane (c-C$_4$F$_8$), for which the GWP is known (3M company-internal analysis cited by Pruette et al. (2000)). A Material Safety Data Sheet for PFG-3480 (trade name for c-C$_4$F$_8$O), lists a GWP of 13 900 (100-yr time horizon) and a lifetime of <4 000 years (3M Company, 2007). It is unknown

30 to us how these results were obtained. In addition, no atmospheric measurements or emissions estimates to the atmosphere are presently available for c-C$_4$F$_8$O.

The present study aims to improve our knowledge on the chemical and radiative properties of c-C$_4$F$_8$O relevant to determining its atmospheric lifetime and to provide the first atmospheric measurements from which we derive estimated global emissions to the atmosphere. Measurements were made on atmospheric samples archived in canisters and Antarctic firn, and

in modern air from in situ observations. From the derived historical record, emissions are estimated using a 12-box chemical transport model of the atmosphere (Cunnold et al., 1983; Rigby et al., 2013; Vollmer et al., 2016). We also conducted laboratory experiments to determine the infrared and ultraviolet (UV) absorption spectra of c-C_4F_8O, and the rate coefficient for the $O(^1D)$ + c-C_4F_8O reaction to estimate the atmospheric lifetime and GWP of c-C_4F_8O.

2 Methods

2.1 c-C_4F_8O in air samples

2.1.1 Measurements of c-C_4F_8O in archived and ambient in situ air

For the present study, archived and urban ambient air samples were analyzed at the Commonwealth Scientific and Industrial Research Organization (CSIRO) laboratory at Aspendale (Victoria, Australia) using Medusa gas chromatographic (GC) mass spectrometric (MS) techniques (Miller et al., 2008). The archived air samples consisted primarily of the Cape Grim Air Archive (CGAA) samples collected under clean air baseline conditions for archival purposes since 1978 at the Cape Grim Baseline Air Pollution Station (Tasmania, Australia 40.7°S, 144.7°E). These >100 samples were collected into 34 L internally electropolished stainless steel canisters (Essex Industries, USA) using cryogenic techniques (Fraser et al., 1991; Langenfelds et al., 1996, 2014; Fraser et al., 2016). The CGAA record was complemented with a few samples collected in the Northern Hemisphere mostly using oil-free diving compressors.

Two firn air samples were also analyzed, which were collected at the Aurora Basin North (ABN) site in Antarctica (71.1°S, 111.4°E). The site is located 550 km inland from Australia's Casey station, at 2710 masl and has a low mean annual air temperature of −44°C. Samples were collected in December 2013; those for the halocarbon measurements were collected into internally electropolished stainless steel containers using a 2-stage teflon-coated viton diaphragm pump.

In situ measurements of c-C_4F_8O at Aspendale (38.0°S, 145.1°E) were started in February 2017. These samples are collected from the rooftop at CSIRO (at 11 m height from the ground) through a 3/8" OD Synflex 1300 tube (Saint-Gobain, France) using a continuous flow air sampling module (Miller et al., 2008) with a diaphragm sampling pump fitted with stainless steel heads and a neoprene membrane (KNF Neuberger, Germany).

All archived air samples were analyzed on the Medusa-GCMS "Medusa-9" in December 2016. The instrument is based on the original design of the Medusa-GCMS used in the Advanced Global Atmospheric Gases Experiment (AGAGE) network (Miller et al., 2008; Prinn et al., 2018) but fitted with different chromatography columns (Vollmer et al., 2018). A GS-GasPro main capillary column (0.32 mm ID × 60 m, Agilent Technologies) was used for the main separation and a column of the same type (5 m) was fitted as a precolumn, allowing for a backflushing of late eluting compounds. In this GCMS setup (Agilent 6890 GC, 5975 MS) c-C_4F_8O was identified using a multi-component diluted mixture of known composition with the MS in scan and selected ion modes. The choice for the two fragments used in the analysis of our air samples was based on the mass spectrum, which we measured for c-C_4F_8O, to the best of our knowledge the first one published for this compound (see Supplement).

Analytes from the samples were cryogenically preconcentrated on a first microtrap of the GCMS and subsequently transferred to a second microtrap, both filled with HayeSepD and held at $\sim -155\,°C$. During this process, water vapor was largely removed using nafion dryers; nitrogen, oxygen, and a large fraction of noble gases were removed due to their trap breakthroughs, and carbon dioxide was removed using a molecular sieve (4A) packed column between the traps. To enhance the

5   signal size of the measured compounds, 3 L sample sizes were used for each measurement (compared to normally 2 L) and the MS electron multiplier voltage was increased by 50 V compared to what was given by the autotune algorithm. Analysis of a single sample lasted 65 min. Archived air sample measurements were bracketed by measurements of a standard (E-146S) to track and correct for MS sensitivity changes. This standard was air compressed into a 34 L tank at the remote Rigi-Seebodenalp station (Switzerland) using an oil-free compressor and was additionally spiked with small amounts of c-C_4F_8O and other com-

10   pounds to enhance the GCMS peak size and signal-to-noise ratio. In general, three measurements of each archived air sample were made. For some, no standard measurement was made between the second and third sample to assess potential memory effects of the system. For c-C_4F_8O, no memory effect and no signal in the blank runs could be detected. Detection limits are estimated at 5 ppq (parts per quadrillion, femtomol mol^{-1}). Mean precisions (2σ) for the measurements of the archived air samples ranged 3–4 ppq (20–5 %) for the low ($\sim$15 ppq) to high ($\sim$70 ppq) mole fractions, respectively. Based on two dif-

15   ferent types of experiments, a linear system response for the relevant mole fraction range was found (see Supplement). In situ urban air measurements at Aspendale are based on 2 L samples and without alteration of the MS electron multiplier voltage. Consequently the precisions are slightly poorer for these measurements. These air precisions were estimated at $\sim$12 ppq ($\sim$17 %, 2σ) under the assumption that c-C_4F_8O remains constant in the air measured in situ at Aspendale on a daily basis.

2.1.2   Absolute calibration and uncertainty estimates for air measurements

20   A primary calibration scale was prepared based on a commercially obtained multi-component mixture in dry synthetic air (Carbagas, Switzerland, HCP-04Carba), with a mole fraction of c-C_4F_8O at 10 ppm (parts-per-million, μmol mol^{-1}). This mixture was diluted manometrically and using a bootstrap technique, resulting in a primary calibration standard (EP-001) with c-C_4F_8O at 1.81 ppt (parts-per-trillion, picomol mol^{-1}). Three secondary standards were additionally prepared from ambient air compressed into cylinders (Essex Industries, USA) and spiked with small quantities of c-C_4F_8O resulting in mole fractions

25   of $\sim$0.5 ppt. These secondary standards were the base for propagating the calibration scale to other calibration standards, in particular that used for the Cape Grim Air Archive measurements (E-146S). They define the Empa-2013 calibration scale for c-C_4F_8O on which our results are reported. The systematic uncertainty of the preparation of this primary calibration scale (including its propagation to the working standards), which defines its accuracy, is estimated at 15 % (2σ). Details of the dilution technique and the primary calibration scale are provided by Vollmer et al. (2015).

2.2 Models and inversion

2.2.1 Firn model

We use a numerical firn air model (Trudinger et al., 1997, 2013) to quantify the movement of c-C_4F_8O in firn air in order to determine the time period for which c-C_4F_8O in the firn samples is representative of the atmosphere. Vertical diffusion in the

5 firn and other physical processes cause a tracer in a firn air sample to correspond to an age spectrum relative to the atmosphere, rather than a discrete age. Green's functions from the firn model represent the age spectrum of a tracer in each firn sample, and are used in this work to relate the measured mole fractions of c-C4F8O in firn to the time-range of the corresponding atmospheric mole fractions.

For ABN, the firn model uses an accumulation rate of $97 \, \mathrm{kg \, m^{-2} \, yr^{-1}}$, a temperature of $-44°C$ and pressure of 695 hPa. The

10 density profile used was based on a spline fit to density measurements. Diffusion parameters in the firn model are calibrated for the ABN site using 12 tracers at between 5 and 11 depths each throughout the firn. Vertical diffusion in the firn and other physical processes cause a firn air sample to correspond to an age spectrum rather than a discrete age. Green's functions from the firn model represent the age spectrum of each firn sample, and are used in this work to relate the measured mole fractions to the time-range of the corresponding atmospheric mole fractions. The diffusion coefficient used in this work for c-C_4F_8O in

15 air relative to CO_2 in air (for a temperature of 253 K) is 0.460. This value was determined using Equation 4 from Fuller et al. (1966) with Le Bas volume increments (e.g. Table 1.3.1, Mackay et al. (2006)) and a multiplier for the Le Bas increments of 0.97 (this value minimizes the difference of calculated relative diffusion coefficients of a number of compounds from values measured by Matsunaga et al. (1993, 2002, 2005)).

2.2.2 12-box atmospheric model

20 We use the AGAGE 12-box atmospheric model (Rigby et al., 2013) to relate the atmospheric mole fractions to surface emissions. Briefly, in this model, the atmosphere is divided into four zonal bands, separated at the equator and at the 30° latitudes, thereby creating boxes of similar air masses. There are also vertical separations, at altitudes represented by 500 hPa and 200 hPa, resulting in the overall 12 boxes. Model transport parameters and stratospheric photolytic loss vary seasonally and repeat interannually (Rigby et al., 2013). We anticipate that variations in emissions dominate atmospheric trends, particularly over

25 the longer (multi-annual) timescales that are our primary focus, so inter-annual variation in transport is not expected to be important here.

2.2.3 Global inversions

To estimate global emissions to the atmosphere from the mole fraction measurements, we employ an inverse calculation (inversion InvE2 from Trudinger et al. (2016), and termed "CSIRO" inversion in Vollmer et al. (2016, 2018)) that was developed

30 to focus on sparse observations from air archives, and firn air and ice core samples that are associated with age spectra. The inversion uses Green's functions from both the firn model and AGAGE 12-box atmospheric model described above to relate firn

and tropospheric mole fraction to c-C_4F_8O surface emissions. The Green's functions from the 12-box model were calculated using a constant distribution of emissions into the four zonal boxes at the surface, and for this we used the relative contributions 0.675, 0.325, 0.0, and 0.0, in the northern-most to southern-most zonal bands. Results are fairly insensitive to emissions distributions that have all emissions in the Northern Hemisphere (see Supplement). The characteristics of sparse atmospheric, firn

5 and ice core data necessitate the use of constraints on the inversion to avoid unrealistic oscillations in the reconstructed mole fractions or negative values of mole fraction or emissions. The inversion uses non-negativity constraints and favors relatively small changes in annual emissions between adjacent years over large, unrealistic fluctuations. A prior emissions history is needed as a starting point for the inversion, then a non-linear constrained optimization method (*contrained_min* routine in IDL (Exelis Visual Information Solutions, Boulder, Colorado)) is used to find the solution that minimizes a cost function consisting

10 of the model-data mismatch weighted by the observation uncertainties, plus the sum of the year-to-year changes in emissions (Trudinger et al., 2016). Given the lack of industry-based bottom-up emission estimates for c-C_4F_8O, we use emissions derived from observations, of perfluorooctane, which was found present for many decades and at low abundances in the global atmosphere (Ivy et al., 2012). Because the prior is not based on information on c-C_4F_8O, we do not include the prior in the cost function. The emissions derived from the inversion are rather insensitive to the choice of the prior (see Supplement), because

15 the prior is used here as a starting point for the inversion only, and not as a constraint. Our observations used in the inversion are the firn measurements and annual values of mole fraction from a smoothing spline fit (50 % attenuation at 10 years) to measurements of the CGAA and in situ measurements at Aspendale. Northern Hemisphere measurements were compared with the reconstructed mole fractions for that hemisphere, but were not used in the inversion. Uncertainties for the CGAA and Aspendale annual means are estimated using a bootstrap method that incorporates temporally-correlated data (see Supplement),

20 uncertainty in firn measurements, uncertainty in the calibration scale of ±15 % and uncertainties in the firn model parameters through the use of an ensemble of firn Green's functions.

2.3 Laboratory studies

Laboratory studies to measure the infrared and UV spectra of c-C_4F_8O and the rate coefficient for the $O(^1D) + c$-C_4F_8O reaction were conducted at the Chemical Sciences Division Laboratories at the National Oceanic and Atmospheric Administration

25 (NOAA), Boulder, Colorado, USA. The apparatus and methods used in this work are described separately below.

2.3.1 Absorption spectra

Absorption spectra were quantified using Beer's law

$$A(\lambda) = -ln\left(\frac{I(\lambda)}{I_0(\lambda)}\right) = \sigma(\lambda) \times L \times [c\text{-}C_4F_8O] \tag{I}$$

where A is the measured absorbance at wavelength λ, $I(\lambda)$ and $I_0(\lambda)$ are the measured light intensities with and without

30 the sample present in the absorption cell, respectively, L is the optical absorption path length, $\sigma(\lambda)$ is the infrared or UV cross section of c-C_4F_8O, and [c-C_4F_8O] is the concentration of c-C_4F_8O. In total, 11 independent absorption spectrum

measurements were used in the linear least-squares fit. The c-C_4F_8O concentration was determined using the ideal gas law and absolute pressure measurements of either the pure compound or of a dilute mixture of the compound in a helium (He) bath gas.

The c-C_4F_8O sample was obtained from SynQuest Laboratories (Inc., Alachua, Florida, USA, 99 % purity). For the experiments described below, c-C_4F_8O was introduced into the absorption cells as a pure sample or in a dilute mixture prepared

5   off-line. The dilute mixtures of c-C_4F_8O in a He (UHP, 99.999 %) bath gas was prepared manometrically in a 12 L Pyrex bulb with an estimated accuracy of $\sim$1 %. Pressures were measured with 100 Torr and 1 000 Torr (130 and 1 300 hPa, respectively) capacitance manometers. Quoted uncertainties are 2σ.

Infrared absorption spectra were measured at 296 K using Fourier transform infrared (FTIR) spectroscopy over the 500–4 000 cm^{-1} spectral region at 1 cm^{-1} resolution with Boxcar apodization. The apparatus has been used extensively in previous

10   studies (Bernard et al., 2017, 2018a). The FTIR was coupled to a 15 cm path length single pass absorption cell with potassium bromide (KBr) windows. A liquid-nitrogen cooled HgCdTe/B semiconductor detector was used. Infrared spectra were recorded in 100 or 500 co-added scans. Absorption spectra were recorded under static conditions using a dilute mixture of c-C_4F_8O in He with a 0.00180 mixing ratio. The c-C_4F_8O concentration used in the absorption measurements was in the range 1.75×10^{15} to 2.34×10^{16} molecule cm^{-3}. Integrated band strengths (IBS) were obtained from the measurement of 11 individual IR spectra.

15   The UV absorption spectrum of c-C_4F_8O was measured at 296 K using a 0.5 m spectrometer equipped with a charge-coupled device (CCD) detector. The collimated output of a 30 W deuterium lamp passed through a 100 cm long and 2.5 cm diameter Pyrex absorption cell with quartz windows. Spectral measurements were made over the wavelength region 200–350 nm. The wavelength scale of the spectrometer was calibrated using the emission lines from a low-pressure Hg pen-ray lamp. c-C_4F_8O was added to the absorption cell in pure form from the original sample. Measurements were performed over a

20   range of c-C_4F_8O concentrations from 2.51×10^{18} to 2.16×10^{19} molecule cm^{-3}. Eleven independent UV absorption spectrum measurements were used in the final linear least-squares fit.

2.3.2   O(^{1}D) reaction rate coefficient

The reactive rate coefficient, k_R, for the reaction

$$O(^1D) + c\text{-}C_4F_8O \quad\quad \rightarrow Products \tag{1a}$$

25
$$O(^1D) + c\text{-}C_4F_8O \quad \rightarrow c\text{-}C_4F_8O + O(^3P) \tag{1b}$$

i.e., the channel resulting in the loss of c-C_4F_8O, was measured at 294 K using a relative method (e.g. Baasandorj et al., 2013). The loss of c-C_4F_8O was measured relative to the loss of the reference compound CHF$_3$ during the same experiment:

$$O(^1D) + CHF_3 \quad\quad \rightarrow Products \tag{2a}$$

$$O(^1D) + CHF_3 \quad \rightarrow CHF_3 + O(^3P) \tag{2b}$$

30   The recommended total rate coefficient for reaction 2, k_2 is $(9.60\pm0.5)\times10^{-12}$ cm^3 molecule^{-1} s^{-1} and the recommended reactive channel branching ratio, k_{2a}/k_2 is 0.25, i.e., $k_{2a} = 2.4\times10^{-12}$ cm^3 molecule^{-1} s^{-1} (Burkholder et al., 2015).

Provided c-C_4F_8O and the reference compound are removed solely by reaction with $O(^1D)$, the rate coefficient for reaction 1a is related to the reference compound rate coefficient by the equation

$$ln\left(\frac{[c\text{-}C_4F_8O]_0}{[c\text{-}C_4F_8O]_t}\right) = \frac{k_{c\text{-}C_4F_8O}}{k_{CHF_3}}\left[ln\left(\frac{[CHF_3]_0}{[CHF_3]_t}\right)\right] \tag{II}$$

where $[c\text{-}C_4F_8O]_0$, $[CHF_3]_0$, $[c\text{-}C_4F_8O]_t$, and $[CHF_3]_t$ are the concentrations of c-C_4F_8O and CHF_3 at times t_0 and t, respectively. $k_{c\text{-}C_4F_8O}$ and k_{CHF_3} are the reactive rate coefficients for the reaction of $O(^1D)$ with c-C_4F_8O (1a) and CHF_3 (2a), respectively.

The Pyrex reactor, which was 100 cm long and with a 2.2 cm internal diameter, was coupled with a Teflon circulating pump to an absorption cell where the loss of c-C_4F_8O and CHF_3 was measured using FTIR spectroscopy. The FTIR absorption cell was equipped a multi-pass cell (485 cm path length) with KBr windows. Spectra were recorded in 100 co-adds at a spectral resolution of 1 cm^{-1}.

$O(^1D)$ was produced by KrF (248 nm) excimer pulsed laser photolysis of ozone:

$$O_3 + h\nu\,(248nm) \rightarrow O(^1D) + O_2(^1\Delta) \tag{3a}$$

$$\rightarrow O(^3P) + O_2(^3\Sigma) \tag{3b}$$

The yield of the $O(^1D)$ channel is 0.9 (Burkholder et al., 2015). After thoroughly mixing the gas mixture in the system, a time zero infrared spectrum was recorded. Ozone was then added slowly to the reactor with the photolysis laser and gas circulation on. The photolysis laser fluence was in the range $\sim$2–7.4 mJ cm^{-2} pulse^{-1}. The laser was operated at 10 or 20 Hz. The total pressure in the cell increased during an experiment by $\sim$300 Torr, mostly due to the addition of He carrier gas used to flush ozone into the reactor. Infrared spectra were recorded at regular intervals with approximately 10 spectra recorded over the course of an experiment. Experiments performed separately demonstrated that there was no significant loss of c-C_4F_8O or CHF_3 in the absence of $O(^1D)$ production. The initial c-C_4F_8O and CHF_3 concentrations were in the range 6.4–6.8$\times10^{14}$ molecule cm^{-3} and 4.5–5.0$\times10^{14}$ molecule cm^{-3}, respectively.

3 Results and discussion

3.1 Infrared spectrum

The infrared absorption spectrum of c-C_4F_8O obtained in this study is shown in Fig. 2. Over the range of c-C_4F_8O concentrations used, the spectra obeyed Beer's law with high precision ($\sim$0.2 %). Spectra recorded at different total pressures had identical band shapes, i.e., the spectrum was independent of the total pressure (He bath gas) over the range of 30–400 Torr.

The integrated band strength (IBS) over the spectral region 500–1 500 cm^{-1} was determined to be $(3.21 \pm 0.01) \times 10^{-16}$ cm^2 molecule^{-1} cm^{-1}, where the quoted uncertainty is the precision of the linear least-squares fit of the data to Beer's law (Equation I). The absolute uncertainty in the c-C_4F_8O spectrum includes estimated uncertainties in the optical path length ($\pm$0.5 %), measured absorbance ($\pm$0.005), temperature ($\pm$1 K), and pressure ($\pm$0.2 %). The absolute uncertainty in the total integrated band strength is estimated to be 3 %.

3.2 UV absorption

UV absorption of c-C$_4$F$_8$O was observed between 200 nm and 225 nm, a range that is most critical for calculations of the c-C$_4$F$_8$O atmospheric photolysis rates. The spectrum is continuous, with cross section decreasing monotonically with increasing wavelength. The cross section measurements obeyed Beer's law with values of $(9.2 \pm 3.9) \times 10^{-24}$ and $(4.4 \pm 2.3) \times 10^{-24}$ cm^2 molecule^{-1} cm^{-1} at 200 and 225 nm, respectively. Overall, the cross sections of c-C$_4$F$_8$O were very low, and therefore, the measurements are susceptible to interference from even minor sample impurities. Therefore, we choose to assign a conservative UV cross section of $<2 \times 10^{-23}$ cm^2 molecule^{-1} cm^{-1} over the 200–225 nm range.

3.3 O(^{1}D) reaction

We found the reactivity of c-C$_4$F$_8$O with O(^{1}D) to be low, which makes the determination of an accurate rate coefficient more challenging. The relative rate data are shown in Fig. 3 and tabulated in the Supplement. The precision of the three independent measurements is high with a fit precision of a few percent. However the agreement between the independent measurements is relatively poor. The low conversion of c-C$_4$F$_8$O, <2 %, and the precision of the infrared spectral subtractions are the primary sources of uncertainty in the measurements. The spectral subtraction uncertainty is illustrated by the error bars included in Fig. 3. The average of individual measurements yields a rate coefficient ratio of 0.21±0.07. However, we recommend a conservative upper-limit of 0.5. Using the recommended O(^{1}D) + CHF$_3$ reactive rate coefficient, $(2.41 \pm 0.12) \times 10^{-12}$ cm^3 molecule^{-1} s^{-1} (Burkholder et al., 2015) yields a c-C$_4$F$_8$O reactive rate coefficient of $<1.2 \times 10^{-12}$ cm^3 molecule^{-1} s^{-1}.

3.4 Atmospheric lifetime

The global annually averaged atmospheric lifetime (τ) of c-C$_4$F$_8$O, is defined with respect to the individual partial lifetimes by the relationship:

$$\frac{1}{\tau} = \frac{1}{\tau_{\text{O}(^1\text{D})}} + \frac{1}{\tau_{h\nu}} + \frac{1}{\tau_{\text{Lyman}-\alpha}} + \frac{1}{\tau_{\text{OH}}} \tag{4}$$

where the individual global loss processes are combined to derive the overall global lifetime. In the present analysis, only O(^{1}D), UV photolysis, and Lyman-α terms are considered. The loss of c-C$_4$F$_8$O via reaction with the OH radical is assumed to make a negligible contribution to the global lifetime and consequently we ignore the last term in Equation 4. The laboratory results for the O(^{1}D) reaction and UV photolysis obtained in this study are combined with an estimated Lyman-α lifetime to derive the lifetime utilizing the 2-D atmospheric model calculation parametrizations reported by Bernard et al. (2018b). The O(^{1}D) reaction represents a stratospheric loss process for c-C$_4$F$_8$O with a partial lifetime, $\tau_{\text{O}(^1\text{D})}$, estimated to be $>30\,000$ years. This extremely long lifetime is a result of the low c-C$_4$F$_8$O reactivity combined with the turn-over time of the stratosphere. The UV photolysis lifetime, $\tau_{h\nu}$ is derived from the c-C$_4$F$_8$O UV cross section upper-limit of 10^{-23} cm^2 molecule^{-1} and an assumed quantum yield of unity for the 200–225 nm region, and is $>15\,000$ years. Combining the estimated O(^{1}D) and UV photolysis lifetimes yields an estimated global lifetime for c-C$_4$F$_8$O $>7\,500$ years.

Given the long atmospheric lifetime of c-C_4F_8O in the troposphere and stratosphere, upper atmospheric loss processes may contribute to the global atmospheric lifetime. Here, we consider loss due to Lyman-α photolysis, although other loss processes are possible. To date, the vacuum UV (VUV) absorption spectrum of c-C_4F_8O, which includes the Lyman-α absorption (121.567 nm), has not been reported. It is reasonable to assume a Lyman-α cross section of $\sim10^{-17}$ cm^2 molecule^{-1} for c-C_4F_8O which would be roughly consistent with values for highly fluorinated compounds (SPARC, 2013). The estimated lifetime due to Lyman-α photolysis, $\tau_{\mathrm{Lyman}-\alpha}$, is then $\sim4\,500$ years (a smaller Lyman-α cross section would lead to a longer

5   lifetime). On the basis of these assumptions, Lyman-α photolysis in the lower mesosphere could be the dominant atmospheric loss process for c-C_4F_8O. Including this Lyman-α photolysis lifetime yields a c-C_4F_8O globally averaged atmospheric lifetime of >3 000 years.

3.5   Global warming potential

c-C_4F_8O has strong vibrational absorption bands within the Earth's atmospheric infrared transmission window (Fig. 4). We

10   determine a radiative efficiency for c-C_4F_8O of 0.430 W m^{-2} ppb^{-1} using the parameterization for atmospherically well-mixed compounds given in Hodnebrog et al. (2013). c-C_4F_8O is therefore a potent greenhouse gas. This radiative efficiency is greater than those of HFCs and chlorofluorocarbons (CFCs), which are typically less than 0.3 W m^{-2} ppb^{-1} (Myhre et al., 2013).

The GWP of c-C_4F_8O was calculated using the global atmospheric lifetime lower-limit of 3 000 years and the radiative

15   efficiency determined in this work:

$$\mathrm{GWP(T)} = \frac{\mathrm{RE}_\tau \left(1 - \exp(-\mathrm{T}/\tau)\right)}{\mathrm{M}_{c\text{-}C_4F_8O} \int \mathrm{RF}_{CO_2}(\mathrm{T})} \tag{5}$$

where RE is the radiative efficiency, T is the time horizon (in years), $\mathrm{M}_{c\text{-}C_4F_8O}$ is the molar weight of c-C_4F_8O and RF_{CO_2} is the radiative forcing of CO_2. The GWPs are 8 975, 12 000, and 16 000 for the 20, 100 and 500-year time-horizons. Therefore, c-C_4F_8O is a potent radiative forcing agent due to the combination of its high radiative efficiency and long atmospheric lifetime.

20   The GWPs for c-C_4F_8O are comparable to the values for long-lived perfluorocarbons (PFCs) that have GWP$_{100}$ values in the range 6 300–11 100 (Harris and Wuebbles, 2014).

3.6   Atmospheric observations and emissions of c-C_4F_8O

We observe a general increase of c-C_4F_8O in the atmosphere over the sample period starting in 1978 (Fig. 1). c-C_4F_8O was detectable in all samples but abundances were low in the early record (<20 ppq) until about 1998, when its growth rate increased

25   strongly. Abundances increased rather steadily to 75 ppq in 2015. The growth rate was at a maximum of 4.3 ppq yr^{-1} in 2004 and declined from the maximum to <0.15 ppq yr^{-1} in 2017. Consequently, its abundance has remained relatively constant in the last few years.

The few Northern Hemisphere samples show higher mole fractions compared to the CGAA at similar times, suggesting predominant Northern Hemisphere emissions. The two firn air samples fit well into the CGAA record with the older sample

30   at slightly lower mole fraction than the oldest CGAA samples. This suggests that c-C_4F_8O was below 10 ppq in the Southern

Hemisphere before 1978, however it is impossible to further pin down the first appearance of this compound in the atmosphere and the exact course of the abundance until ∼1980 because our knowledge of c-C_4F_8O prior to the CGAA is based on only one firn measurement with air spanning several decades (see calculated Green's functions in the Supplement). Given that the storage time of the two firn air samples in the canisters is much shorter than those of the older CGAA samples, the good agreement is also supportive of storage stability of c-C_4F_8O in the CGAA tanks and confirms that the observed record is not a

5   simple artifact of degradation of c-C_4F_8O in canisters over time.

In situ measurements at Aspendale, which are available on a regular measurement basis since February 2017, show constant abundances of c-C_4F_8O at ∼74 ppq. This lack of growth is an indication of currently very small, if at all any, emissions of this compound. Also, pollution events are absent from this urban in situ record within the precision of these measurements, suggesting that c-C_4F_8O is not emitted within the airmass footprints of the site.

10   Emissions derived from the atmospheric observations were low during the first part of our record (Fig. 1). Until 1980, when the global mean abundance of c-C_4F_8O was 11 ppq, cumulative emissions had reached 0.4 kt. For the time after ∼1980, when observations became more frequent, emissions were 0.02–0.03 kt yr^{-1} for about a decade. From the mid 1990s, emissions increased strongly to a maximum of 0.16 ($\pm$0.04, 2 σ) kt yr^{-1} in 2004. Surprisingly, emissions have declined since and have reached 0.01 kt yr^{-1} by 2017. This rapid decline is suggestive of a choice for other compounds in large scale industrial

15   application such as in the semiconductor industry. Cumulative emissions until 2017 amount to 2.8 (2.6–3.2) kt. If scaled with the GWP on a 100-yr time horizons, as derived below, they correspond to 34 Mt CO_2-equivalents. Despite the high GWP, these emissions are small compared to the major greenhouse gases but of similar magnitude to some of the other minor greenhouse gases such as minor perfluorocarbons and fluorinated inhalation anesthetics (Ivy et al., 2012; Vollmer et al., 2015). Whether these cumulative emissions remain at low levels will depend on potential future choices for c-C_4F_8O in large scale applications.

20 ## 4   Conclusions

We provide first laboratory experiments of atmospheric loss processes and first atmospheric observations of c-C_4F_8O, a persistent greenhouse gas not regulated by the Montreal and Kyoto Protocols. We measured infrared and UV absorption spectra of c-C_4F_8O, and the rate coefficient for the $O(^1D)$ + c-C_4F_8O reaction. These experimental results suggest that c-C_4F_8O is an atmospherically persistent trace gas with an atmospheric lifetime of >3 000 years. In addition, its strong absorption in the "at-

25   mospheric window" results in a very high radiative efficiency, and when combined with the long atmospheric lifetime, yields a high global warming potential of 12 000 (100-year time horizon), which is exceeded by only a few other synthetic greenhouse gases. We show an increase of c-C_4F_8O in the atmosphere to present mole fractions of ∼74 ppq. Emissions, which were derived from these observations, have strongly declined after a peak in 2004. The reason for this recent decline, and whether this is only a temporary feature, remains speculative. We hypothesize that the emissions decline is a result of the industry's choice

30   for alternative substances for chemical vapor chamber cleaning, which is assumed to have been its primary use in the last two decades. However, even if emissions were completely halted, it will, due to the very long lifetime of c-C_4F_8O, take thousands of years for the compound to be removed from the atmosphere.

Data used in this study are available from the Supplement. Mention of trade names or commercial products does not constitute an endorsement or recommendation by NOAA for use.

Acknowledgements. We acknowledge the station personnel at Cape Grim for flask sampling for the Cape Grim Air Archive (CGAA) project, which is jointly operated by CSIRO and the Australian government Bureau of Meteorology. CSIRO research at Cape Grim is supported by CSIRO, Bureau of Meteorology, the Australian government Department of Environment and Energy, and Refrigerant Reclaim Australia. We gratefully acknowledge the field team and the national research programs that supported the Aurora Basin North drilling project. M. K. V. acknowledges support from the Swiss Federal Office for the Environment (FOEN) within the Swiss National Programs HALCLIM and CLIMGAS, and 2016 grants from Empa and the Swiss National Science Foundation (SNSF) for technical development and archived air and firn air measurements at CSIRO Aspendale. The work at NOAA was supported in part by NOAA's Climate Program Office Atmospheric Chemistry, Carbon Cycle, and Climate Program. General instrument support is provided by members of the Advanced Global Atmospheric Gases Experiment (AGAGE). We acknowledge the contribution by Peter Salameh, who developed and supports GCWerks, a software control system used in the Medusa-GCMS measurements of air samples described here. Matt Rigby is acknowledged for his contributions to the AGAGE 12-box model.

References

3M Company: 3M Material Safety Data Sheet 3M(TM) PFG-3480 Specialty Gas, https://userweb.jlab.org/~brads/c4f8o/c4f8o-3M-msds.pdf, last accessed 15 May 2018, 2007.

Acconcia, T. V., Agócs, A. G., Barile, F., Barnaföldi, G. G., Bellwied, R., Bencédi, G., Bencze, G., Berényi, D., Boldizsár, L., Chattopadhyay, S., Chinellato, D. D., Cindolo, F., Cossyleon, K., Das, D., Das, K., Das-Bose, L., Dash, A. K., D'Ambrosio, S., De Cataldo, G., De Pasquale, S., Di Bari, D., Di Mauro, A., Futó, E., Garcia-Solis, E., Hamar, G., Harton, A., Iannone, G., Jimenez, R. T., Kim, D. W., Kim, J. S., Knospe, A., Kovács, L., Lévai, P., Markert, C., Martinengo, P., Molnár, L., Nappi, E., Oláh, L., Paić, G., Pastore, C., Patimo, G., Patino, M. E., Peskov, V., Pinsky, L., Piuz, F., Pochybová, S., Sgura, I., Sinha, T., Song, J., Takahashi, J., Timmins, A., Van Beelen, J. B., Varga, D., Volpe, G., Weber, M., Xaplanteris, L., Yi, J., and Yoo, I.-K.: VHMPID RICH prototype using pressurized C_4F_8O radiator gas and VUV photon detector, Nucl. Instr. and Meth. A, 767, 50–60, doi:10.1016/j.nima.2014.08.005, 2014.

Artuso, M., Boulahouache, C., Blusk, S., Butt, J., Dorjkhaidav, O., Menaa, N., Moutain, R., Muramatsu, H., Nandakumar, R., Randrianarivony, K., Sia, R., Skwarnicki, T., Stone, S., Wang, J. C., and Zhang, K.: Performance of a C_4F_8O gas radiator ring imaging Cherenkov detector using multi-anode photomultiplier tubes, Nucl. Instr. and Meth. A, 558, 373–387, 2006.

Baasandorj, M., Fleming, E. L., Jackman, C. H., and Burkholder, J. B.: O(^{1}D) kinetic study of key ozone depleting substances and greenhouse gases, J. Phys. Chem. A, 117, 2434–2445, doi:10.1021/jp312781c, 2013.

Bernard, F., Papanastasiou, D. K., Papadimitriou, V. C., and Burkholder, J. B.: Infrared absorption spectra of linear (L2–L5) and cyclic (D3–D6) permethylsiloxanes, J. Quant. Spectrosc. Radiat. Transf., doi:10.1016/j.jqsrt.2017.08.006, 2017.

Bernard, F., Papanastasiou, D. K., Papadimitriou, V. C., and Burkholder, J. B.: Infrared absorption spectra of N(C_xF_{2x+1})$_3$, x=2–5 perfluoroamines, J. Quant. Spectrosc. Radiat. Transf., doi:10.1016/j.jqsrt.2018.02.039, 2018a.

Bernard, F., Portmann, R. W., Papanastasiou, D. K., and Burkholder, J. B.: Atmospheric loss processes and global warming potentials for perfluoroamines: N(C_xF_{2x+1})$_3$, x=3–5, in preparation, 2018b.

Beu, L. S.: Reduction of Perfluorocompound (PFC) Emissions: 2005 State-of-the-Technology Report, International SEMATECH Manufacturing Initiative Technology Transfer #05104693A-ENG, Semiconductor Manufacturing Technology, SEMATECH, Austin, TX 78741, U.S.A., http://ismi.sematech.org, 2005.

Burkholder, J. B., Sander, S. P., Abbatt, J., Barker, J. R., Huie, R. E., Kolb, C. E., Kurylo, M. J., Orkin, V. L., Wilmouth, D. M., and Wine, P. H.: Chemical Kinetics and Photochemical Data for Use in Atmospheric Studies, Evaluation No. 18 of the NASA Panel for Data Evaluation, JPL Publication 15-10, Jet Propulsion Laboratory, Pasadena, http://jpldataeval.jpl.nasa.gov, 2015.

Carpenter, L. J. and Reimann, S.: Ozone-Depleting Substances (ODSs) and Other Gases of Interest to the Montreal Protocol, Chapter 1, in: Scientific Assessment of Ozone Depletion: 2014, Global Ozone Research and Monitoring Project — Report No. 55, World Meteorological Organisation, Geneva, Switzerland, 2014.

Chachereau, A., Fedor, J., Janečková, R., Kočíšek, J., Rabie, M., and Franck, C. M.: Electron attachment properties of c-C_4F_8O in different environments, J. Phys. D: Appl. Phys., 49, doi:10.1088/0022-3727-49-37-375201, 2016.

Cunnold, D. M., Prinn, R. G., Rasmussen, R. A., Simmonds, P. G., Alyea, F. N., Cardelino, C. A., Crawford, A. J., Fraser, P. J., and Rosen, R. D.: The atmospheric lifetime experiment 3. Lifetime methodology and application to 3 years of $CFCl_3$ data, J. Geophys. Res., 88, 8379–8400, doi:10.1029/JC088iC13p08379, 1983.

Dahl, D. A., Rabie, M., Häfliger, P., and Franck, C. M.: Electron attaching properties of c-C_4F_8O derived from swarm parameter measurements in buffer gases, In Proceedings of the Gas Discharge (GD) 2014, Orléans, France, July 6 – 11, 2014.

Favre, H. A. and Powell, W. H.: Nomenclature of Organic Chemistry, IUPAC Recommendations and Preferred Names 2013, The Royal Society of Chemisty, Cambridge, UK, 2014.

Fraser, P. J. Steele, L. P., Pearman, G. I., Coram, S., Derek, N., Langenfelds, R. L., and Krummel, P. B.: Non-carbon dioxide greenhouse gases at Cape Grim: a 40 year odyssey, Baseline Atmospheric Program (Australia) History and Recollections, 2016, 45–76, 2016.

Fraser, P. J., Langenfelds, R. L., Derek, N., and Porter, L. W.: Studies in archiving techniques, vol. 1989, pp. 16–29, Department of the Arts, Sport, the Environment, Tourism and Territories, Bureau of Meteorology and CSIRO Division of Atmospheric Research, Canberra, Australia, 1991.

Frick, H. R. and Anderson, R. W.: Preparation of Octafluorotetrahydrofuran, https://patents.google.com/patent/US3679709, US Patent 3,679,709, 1972.

Fuller, E. N., Schettler, P. D., and Giddings, J. C.: A new method for prediction of binary gas-phase diffusion coefficients, Ind. Eng. Chem., 58, 19–27, 1966.

Harris, N. R. P. and Wuebbles, D. J.: Scenarios and information for policymakers, Chapter 5, in: Scientific Assessment of Ozone Depletion: 2014, Global Ozone Research and Monitoring Project — Report No. 55, World Meteorological Organisation, Geneva, Switzerland, 2014.

Hodnebrog, Ø., Etminan, M., Fuglestvedt, J. S., Marston, G., Myhre, G., Nielsen, C. J., Shine, K. P., and Wallington, T. J.: Global warming potentials and radiative efficiencies of halocarbons and related compounds: A comprehensive review, Rev. Geophys., 51, 300–378, doi:10.1002/rog.20013, 2013.

Ivy, D. J., Rigby, M., Baasandorj, M., Burkholder, J. B., and Prinn, R. G.: Global emission estimates and radiative impact of C_4F_{10}, C_5F_{12}, C_6F_{14}, C_7F_{16} and C_8F_{18}, Atmos. Chem. Phys., 12, 7635–7645, doi:10.5194/acp-12-7635-2012, 2012.

Kim, J. H., Bae, J. W., Oh, C. H., Kim, K. J., Lee, N. E., and Yeom, G. Y.: C_4F_8O/O_2/N-based additive gases for silicon nitride plasma enhanced chemical vapor deposition chamber cleaning with low global warming potentials, Jpn. J. Appl. Phys., 41, 6570–6573, 2002.

Kim, K. J., Oh, C. H., Lee, N.-E., Kim, J. H., Bae, J. W., Yeom, G. Y., and Yoon, S. S.: Global warming gas emission during plasma cleaning process of silicon nitride using c-C_4F_8O chemistry with additive Ar and N_2, J. Vac. Sci. Technol. B, 22, 483–488, 2004.

Langenfelds, R. L., Fraser, P. J., Francey, R. J., Steele, L. P., Porter, L. W., and Allison, C. E.: The Cape Grim air archive: The first seventeen years, 1978–1995, in: Baseline Atmospheric Program (Australia) 1994-95, edited by Francey, R. J., Dick, A. L., and Derek, N., pp. 53–70, Bureau of Meteorology and CSIRO Division of Atmospheric Research, Australian Bureau of Meteorology and CSIRO Marine and Atmospheric Research, Melbourne, Australia, 1996.

Langenfelds, R. L., Krummel, P. B., Fraser, P. J., Steele, L. P., Ward, J., and Somerville, N. T.: Archiving of Cape Grim air, in: Baseline Atmospheric Program Australia 2009-2010, edited by Derek, N., Krummel, P. B., and Cleland, S. J., pp. 44–45, Australian Bureau of Meteorology and CSIRO Marine and Atmospheric Research, Melbourne, Australia, 2014.

Mackay, D., Shiu, W.-Y., and Ma, K.-C., eds.: Illustrated Handbook of Physical-chemical Properties and Environmental Fate for Organic Chemicals, 2006.

Matsunaga, N., Hori, M., and Nagashima, A.: Mutual diffusion coefficients of halogenated-hydrocarbon refrigerant-air systems, in: High Temperatures – High Pressures, 13 ECTP Proceedings, vol. 25, pp. 63–70, 1993.

Matsunaga, N., Hori, M., and Nagashima, A.: Measurements of the mutual diffusion coefficients of gases by the Tylor method (7th report, measurements on the SF_6-air SF_6-N_2, SF_6-O_2, CFC12-N_2, CFC12-O_2, HCFC22-N_2 and HCFC22-O_2 systems), Trans. Jpn. Soc. Mech. Eng. B., 68, 550–555, 2002.

Matsunaga, N., Hori, M., and Nagashima, A.: Measurements of the mutual diffusion coefficients of carbon tetrafluoride and methyl bromide in air, nitrogen and oxygen, in: Proc. 26th Jpn. Symp. Therm. Props, vol. 26, pp. 499–501, 2005.

McCoy, M.: Booming semiconductor business smiles on chemical suppliers, Chemical and Engineering News, 78, 23–24, doi:10.1021/cen-v078n030.p023, 2000.

Miller, B. R., Weiss, R. F., Salameh, P. K., Tanhua, T., Greally, B. R., Mühle, J., and Simmonds, P. G.: Medusa: A sample preconcentration and GC/MS detector system for in situ measurements of atmospheric trace halocarbons, hydrocarbons, and sulfur compounds, Anal. Chem., 80, 1536–1545, doi:10.1021/ac702084k, 2008.

Myhre, G., Shindell, D., Breon, F.-M., Collins, W., Fuglestvedt, J., Huang, J., Koch, D., Lamarque, J.-F., Lee, D., Mendoza, B., Nakajima, T., Robock, A., Stephens, G., Taekmura, T., and Zhang, H.: Anthropogenic and Natural Radiative Forcing, in: Climate Change 2013: The Physical Science Basis. Contribution of Working Group I to the Fifth Assessment Report of the Intergovernmental Panel on Climate Change, edited by Stocker, T. F., Qin, D., Plattner, G.-K., Tignor, M., Allen, S. K., Boschung, J., Nauels, A., Xia, Y., Bex, V., and Midgley, P. M., Cambridge University Press, Cambridge, United Kingdom and New York, NY, USA, 2013.

Oh, B. H., Bae, J. W., Kim, J. H., J., K. K., Ahn, Y. S., Lee, N.-E., Yeom, G. Y., Yoon, S. S., Chae, S.-K., Ku, M.-S., Lee, S.-G., and Cho, D.-H.: Effect of $O_2(CO_2)/C_4F_8O$ gas combinations on global warming gas emission in silicon nitride PECVD plasma cleaning, Surface and Coatings Technology, 146-147, 522–527, 2001.

Prinn, R. G., Weiss, R. F., Arduini, J., Arnold, T., DeWitt, H. L., Fraser, P. J., Ganesan, A. L., Gasore, J., Harth, C. M., Hermansen, O., Kim, J., Krummel, P. B., Li, S., Loh, Z. M., Lunder, C. R., Maione, M., Manning, A. J., Miller, B. R., Mitrevski, B., Mühle, J., O'Doherty, S., Park, S., Reimann, S., Rigby, M., Saito, T., Salameh, P. K., Schmidt, R., Simmonds, P. G., Steele, L. P., Vollmer, M. K., Wang, R. H., Yao, B., Yokouchi, Y., Young, D., and Zhou, L.: History of chemically and radiatively important atmospheric gases from the Advanced Global Atmospheric Gases Experiment (AGAGE), Earth System Science Data, 10, 985–1018, doi:10.5194/essd-10-985-2018, https://www.earth-syst-sci-data.net/10/985/2018/, 2018.

Pruette, L., Karecki, S., Reif, R., Tousignant, L., Reagan, W., Kesari, S., and Zazzera, L.: Evaluation of C_4F_8O as an alternative plasma-enhanced chemical vapor deposition chamber cleaning chemistry, J. Electrochem. Soc., 147, 1149–1153, doi:10.1149/1.1393328, 2000.

Rigby, M., Prinn, R. G., O'Doherty, S., Montzka, S. A., McCulloch, A., Harth, C. M., Mühle, J., Salameh, P. K., Weiss, R. F., Young, D., Simmonds, P. G., Hall, B. D., Dutton, G. S., Nance, D., Mondeel, D. J., Elkins, J. W., Krummel, P. B., Steele, L. P., and Fraser, P. J.: Re-evaluation of lifetimes of the major CFCs and CH_3CCl_3 using atmospheric trends, Atmos. Chem. Phys., 13, 2691–2702, doi:10.5194/acp-13-2691-2013, 2013.

SPARC: SPARC Report on the Lifetimes of Stratospheric Ozone-Depleting Substances, Their Replacements, and Related Species, Tech. Rep. 6, WCRP-15/2013, 2013.

Trudinger, C. M., Enting, I. G., Etheridge, D. M., Francey, R. J., Levchenko, V. A., Steele, L. P., Raynaud, D., and Arnaud, L.: Modeling air movement and bubble trapping in firn, J. Geophys. Res., 102, 6747–6763, doi:10.1029/96JD03382, 1997.

Trudinger, C. M., Enting, I. G., Rayner, P. J., Etheridge, D. M., Buizert, C., Rubino, M., Krummel, P. B., and Blunier, T.: How well do different tracers constrain the firn diffusivity profile?, Atmos. Chem. Phys., 13, doi:10.5194/acp-13-1485-2013, 2013.

Trudinger, C. M., Fraser, P. J., Etheridge, D. M., Sturges, W. T., Vollmer, M. K., Rigby, M., Martinierie, P., Mühle, J. Worton, D. R., Krummel, P. B., Steele, L. P., Miller, B. R., Laube, J., Mani, F., Rayner, P. J., Harth, C. M., Witrant, E., Blunier, T., Schwander, J., O'Doherty, S., and Battle, M.: Atmospheric abundance and global emissions of perfluorocarbons CF_4, C_2F_6 and C_3F_8 since 1800 inferred from ice core, firn, air archive and in situ measurements, Atmos. Chem. Phys., 16, 11733–11754, doi:10.5194/acp-16-11733-2016, 2016.

United Nations: Montreal Protocol on Substances That Deplete the Ozone Layer. Montreal, 16 September 1987. Amendment to the Montreal Protocol on Substances That Deplete the Ozone Layer, Kigali, 15 October 2016, Tech. Rep. C.N.872.2016.TREATIES-XXVII.2.f (Depositary Notification), United Nations, New York, 10017, 2016.

Vollmer, M. K., Rhee, T. S., Rigby, M., Hofstetter, D., Hill, M., Schoenenberger, F., and Reimann, S.: Modern inhalation anesthetics: Potent greenhouse gases in the global atmosphere, Geophys. Res. Lett., 42, 1606–1611, doi:10.1002/2014GL062785, 2015.

Vollmer, M. K., Mühle, J., Trudinger, C. M., Rigby, M., Montzka, S. A., Harth, C. M., Miller, B. R., Henne, S., Krummel, P. B., Hall, B. D., Young, D., Kim, J., Arduini, J., Wenger, A., Yao, B., Reimann, S., O'Doherty, S., Maione, M., Etheridge, D. M., Li, S., Verdonik, D. P.,
10   Park, S., Dutton, G., Steele, L. P., Lunder, C. R., Rhee, T. S., Hermansen, O., Schmidbauer, N., Wang, R. H. J., Hill, M., Salameh, P. K., Langenfelds, R. L., Zhou, L., Blunier, T., Schwander, J., Elkins, J. W., Butler, J. H., Simmonds, P. G., Weiss, R. F., Prinn, R. G., and Fraser, P. J.: Atmospheric histories and global emissions of halons H-1211 ($CBrClF_2$), H-1301 ($CBrF_3$), and H-2402 ($CBrF_2CBrF_2$), J. Geophys. Res. Atmos., 121, 3663–3686, doi:10.1002/2015JD024488, 2016.

Vollmer, M. K., Young, D., Trudinger, C. M., Mühle, J., Henne, S., Rigby, M., Park, S., Li, S., Guillevic, M., Mitrevski, B., Harth, C. M., Miller, B. R., Reimann, S., Yao, B., Steele, L. P., Wyss, S. A., Lunder, C. R., Arduini, J., McCulloch, A., Wu, S., Rhee, T. S., Wang, R. H. J., Salameh, P. K., Hermansen, O., Hill, M., Langenfelds, R. L., Ivy, D., O'Doherty, S., Krummel, P. B., Maione, M., Etheridge, D. M., Zhou, L., Fraser, P. J., Prinn, R. G., Weiss, R. F., and Simmonds, P. G.: Atmospheric histories and emissions of chlorofluorocarbons CFC-13 ($CClF_3$), ΣCFC-114 ($C_2Cl_2F_4$), and CFC-115 (C_2ClF_5), Atmos. Chem. Phys., 18, 979–1002, doi:10.5194/acp-18-979-2018,
470   https://www.atmos-chem-phys.net/18/979/2018/, 2018.
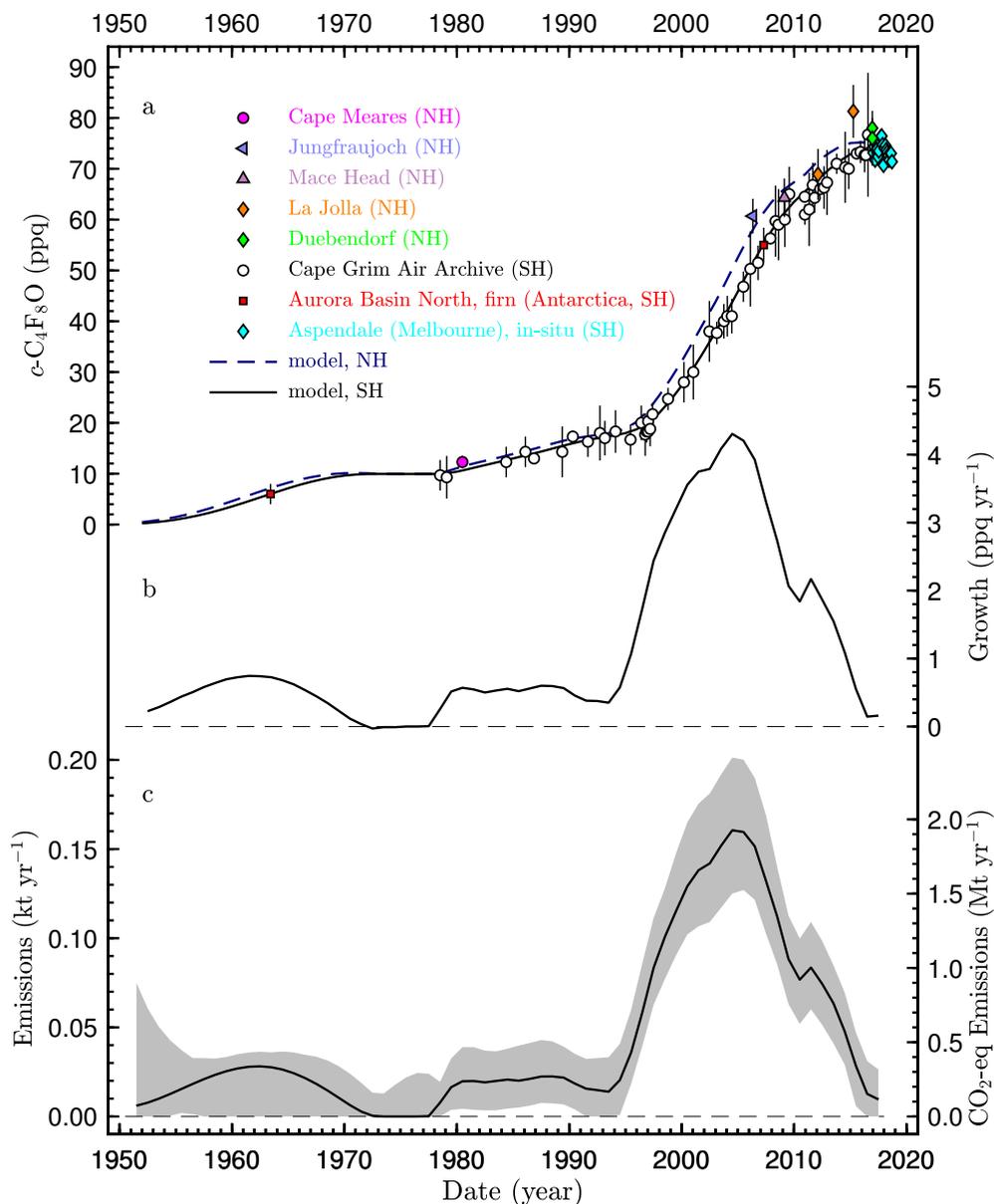
Figure 1. Atmospheric observations (a), growth rates (b), and emissions (c) of octofluorooxolane (octafluorotetrahydrofuran, c-C_4F_8O). Abundances are given as dry air mole fractions in ppq (femtomol mol^{-1}) on the Empa-2013 primary calibration scale. Vertical bars denote the measurement precision (2σ) for the flask samples. Emission uncertainties are 2σ. Samples were collected in the Northern Hemisphere (NH) at Cape Meares (Oregon, 45.5°N, 124.0°W), Jungfraujoch (Switzerland, 46.5°N, 8.0°E), Mace Head (Ireland, 53.3°N, 9.9°W), La Jolla (California, 32.9°N, 117.3°W), and Dübendorf (Switzerland, 47.4°N, 8.6°E). Southern Hemisphere (SH) samples were mainly from the Cape Grim Air Archive collected at Cape Grim (Tasmania, 40.7°S, 144.7°E), two samples from the Aurora Basin North firn air sampling site (Antarctica, 71.2°S, 111.4°E), and in situ monthly means since February 2017 from Aspendale, Victoria, Australia (38.0°S, 145.1°E), with uncertainty bars omitted to aid visual clarity. Emissions are shown on the left y-axis and in CO_2 equivalent emissions based on a global warming potential of 12 000 (100-yr time frame) on the right y-axis.
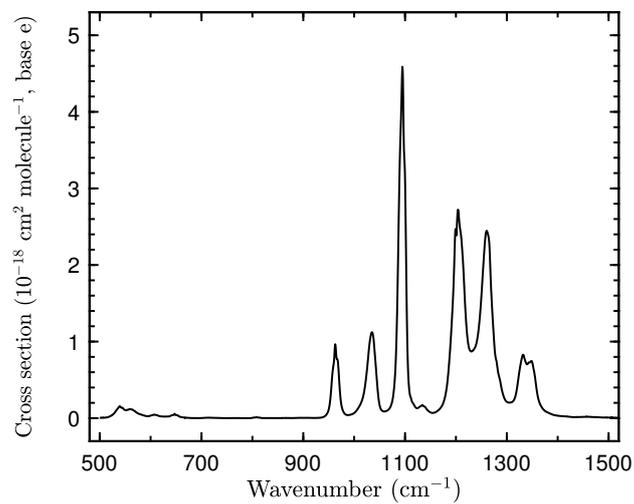
Figure 2. Infrared absorption spectrum of octafluorooxolane (c-C$_4$F$_8$O) measured in this work at 296 K at 1 cm^{-1} resolution.
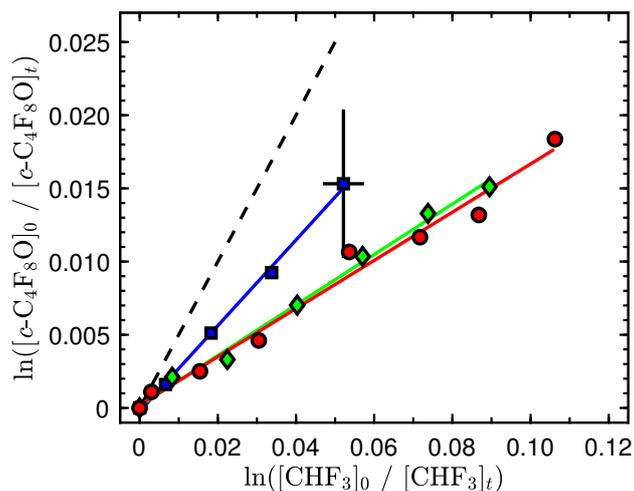
Figure 3. Relative rate data obtained in this work for the O(^{1}D) + c-C$_4$F$_8$O reaction at 296 K. The different symbols are results from independent experiments and the solid lines are linear least-square fits to the data of the individual experiments. Representative estimated error bars from the infrared spectral analysis are included only on a single data point for improved clarity of the graph. The dashed line represents the upper-limit rate coefficient ratio recommended in this work.
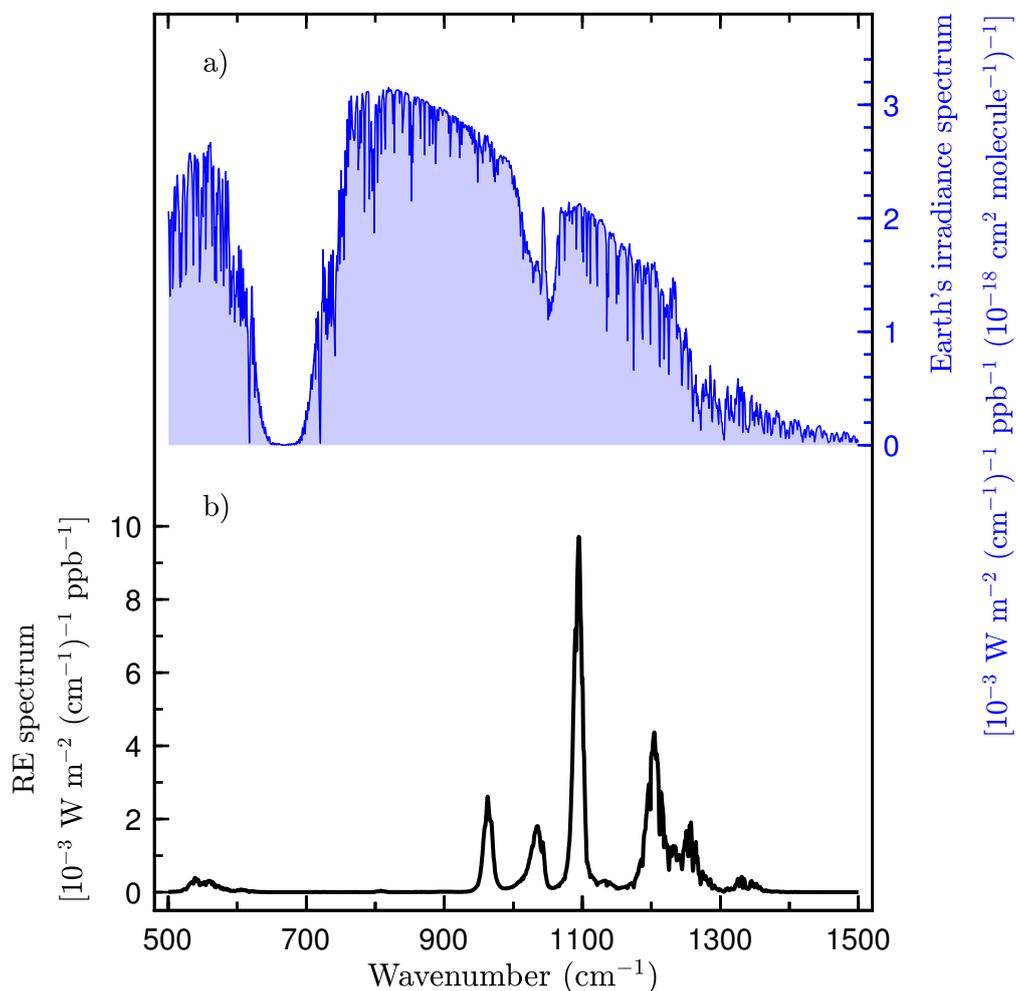
Figure 4. a) Earth's irradiance spectrum as reported by Hodnebrog et al. (2013) and b) radiative efficiency (RE) spectrum of octafluoroox-olane (c-C_4F_8O).